Bayesian Network based causal map generation and root cause identification in complex industrial processes

Kalyani Zope[1], Tanmaya Singhal[2], Sri Harsha Nistala[3], Venkataramana Runkana[4]

[1,2,3,4]TCS Research, Tata Consultancy Services Ltd., Pune – 411013, India

kalyani.zope@tcs.com
tanmaya.singhal@tcs.com
sriharsha.nistala@tcs.com
venkat.runkana@tcs.com

ABSTRACT

Real-time root cause identification (RCI) of faults or abnormal events in industries gives plant personnel the opportunity to address the faults before they progress and lead to failure. RCI in industrial systems must deal with their complex behavior, variable interactions, corrective actions of control systems and variability in faulty behavior. Bayesian networks (BNs) is a data-driven graph-based method that utilizes multivariate sensor data generated during industrial operations for RCI. Bayesian networks, however, require data discretization if data contains both discrete and continuous variables. Traditional discretization techniques such as equal width (EW) or equal frequency (EF) discretization result in loss of dynamic information and often lead to erroneous RCI. To deal with this limitation, we propose the use of a dynamic discretization technique called Bayesian Blocks (BB) which adapts the bin sizes based on the properties of data itself. In this work, we compare the effectiveness of three discretization techniques, namely EW, EF and BB coupled with Bayesian Networks on generation of fault propagation (causal) maps and root cause identification in complex industrial systems. We demonstrate the performance of the three methods on the industrial benchmark Tennessee-Eastman process (TEP). For two complex faults in TEP, the BB with BN method successfully diagnosed correct root causes of the faults, and reduced redundancy (up to 50%) and improved the propagation paths in causal maps compared to the other two techniques.

Keywords: Bayesian Networks, Fault localization, Root cause Identification, Dynamic Discretization

1. INTRODUCTION

Predictive maintenance in manufacturing and process industries is expected to reduce breakdowns/unplanned shutdowns and time to repair critical assets thereby improving the availability of assets and reduce the cost of inventory and maintenance. The emergence of Industrial Internet of Things (IIoT) brought about a renewed interest in predictive maintenance for industries. Real time monitoring, reliable fault detection and diagnosis, estimation of remaining useful life for faulty components and dynamic scheduling of maintenance activities are the key steps in practicing predictive maintenance. Fault diagnosis is an umbrella term that covers identification of key variables/sensors bearing the fault signature (fault localization/isolation), classification of detected fault into one or more known fault classes (fault classification) and detecting the root cause/source of the fault (root cause identification).

Of these, root cause identification (RCI) of faults or abnormal events in real-time or near real-time is a key ask from industries as it enables operators and plant managers to pinpoint the source(s) of the fault and take appropriate corrective actions to prevent catastrophic failure. RCI in industrial systems is, however, complex due to the large number of variables, corrective actions of control systems and wide variability in faulty behavior. It is, therefore, not practical for experts or plant operators to manually localize and identify the root cause of the fault. On the other hand, automatic approaches to root cause identification exist and can be broadly classified into ‘knowledge-based’ and ‘data-driven’ approaches. Knowledge-based methods (such as FMEA) require a priori knowledge of faults and the relationship between faults and observations (Persana & Patel, 2014). While such knowledge can be derived from various sources, the initial effort required for this approach is significant and the gathered knowledge may not be exhaustive leading to missed identifications in some cases.

On the other hand, data-driven methods that utilize historical and current operations data collected from equipment and process sensors can be applied with minimal initial effort. Data-driven techniques for root cause identification such as Granger causality (H. S. Chen, Yan, Zhang, Liu, & Yao, 2018) and Transfer Entropy(TE) (Shu and Zhao 2013) are available in literature. Granger causality is a statistical method that describes a linear causality assuming linear relationship between process variables. It does not capture non-linear relationships and its applicability is limited to stationary time-series data. Transfer Entropy is a model-free theoretical method of causality which does not assume any functional form of variables and analyzes causality between variables based on conditional probability estimation (Zhao, Wang, Chen, Yao, & Xu, 2020). However, accuracy of estimation is dependent on the quantity of data and wherein larger datasets improve accuracy but lead to large computation times. (Wollstadt, Martínez-Zarzuela, Vicente, Díaz-Pernas, & Wibral, 2014). Therefore, TE is not suitable for large datasets. To deal with these limitations, probabilistic models such as Bayesian models have been proposed (Lokrantz, Gustavsson, and Jirstrand 2018; Mechraoui, Medjaher, and Zerhouni 2008; Wang et al. 2018). (Meel et al. 2007) initially used Bayesian networks (BNs) for root cause identification. Learning BNs with a mix of continuous/numeric and categorical variables require discretization of the continuous variables. Traditional discretization methods such as Equal Width (EW) discretization (Kerber 1992) divides the data into fixed number of intervals while Quartile-based discretization divides the data into four parts using 3 quartiles where each part contains 25% of data. These methods, with fixed number of intervals, invariantly lose some amount of dynamic information and affect the Bayesian network inference. It is desired that discretization loses minimal dynamic information contained in the variables and work in an unsupervised manner to maximize the mutual information between all related variables in order to capture the wide range of possible industrial faults (step faults, slow drift, etc.). In this paper, we propose a novel root cause identification approach that combines Bayesian Blocks (BB), a dynamic discretization method based on Bayesian statistics, and Bayesian Networks. We demonstrate the efficacy of the proposed approach on the Tennessee Eastman problem.

The rest of the paper is organized as follows: Bayesian Networks and various discretization methods used in the work are briefly discussed in Section 2. The proposed methodology for fault detection and root cause identification is presented in Section 3. An overview of the Tennessee Eastman benchmark problem is given in Section 4. Application of the proposed methodology to two faults in the Tennessee Eastman process for RCI is demonstrated and discussed in Section 5. Finally, conclusions and future work are given in Section 6.

2. BACKGROUND

2.1. Bayesian Networks

A Bayesian network is a probabilistic graphical model that captures conditional dependencies between variables of interest (Pearl 1988). Bayesian networks are expressed by Directed Acyclic Graphs (DAGs) which represent the joint probability distribution over a set of random variables. Conditional dependencies are represented by edges in the DAG and each node represents a unique random variable. Through these relationships, inference on the random variables can be efficiently conducted and therefore causation. A BN is the pair (S, Θ), where S = (X, E) is a DAG. X is a set of variables (*x1, x2,..., xn*) as nodes and E is a set of connections of X. The graph structure encrypts the following set of independence assumptions: The probability of each variable depends on its parents and independent of all other variables (non-descendants). The second component of the pair Θ, represents the set of parameters that quantifies the network. It gives a set of conditional probability distributions of the variables Xi given their parent nodes Pa in S and represents a unique joint probability distribution over X as,

$$\mathrm{P}(x1, x2 \ldots, xn) = \prod_{i=1}^{n} \mathrm{P}(xi|\mathrm{Pa}(xi)) \quad (1)$$

2.2. Discretization Methods

Discretization transforms numeric data into categorical data. Equal Width discretization (EWD) and Equal Frequency discretization (EFD) are two popular discretization methods that are widely used for transforming numeric data to categorical data. EWD divides the data into equal number of *n* bins. The width of each bin is calculated as $w = (\max - \min)/n$ and the bin bounds are $\min+w$, $\min+2w$, ..., $\min+(n-1)w$. EFD divides data in such a way that the number of values in each bin are the same.

Bayesian Blocks Discretization (BBD) is a dynamic discretization method which adapts the bin sizes based on the properties of data itself. This method optimizes one of several possible fitness functions to determine an optimal binning for data, where the bin sizes are not necessarily equal width. Consider a time series, $\mathrm{s}(t)$ with time interval, $\mathcal{T}$, where $\mathrm{t} = 1,2, \ldots, \mathcal{T}$. The time series can be modelled as:

$$\mathrm{x}(t_n) \equiv x_n = \mathrm{s}(t_n) + z_n \quad (2)$$

Where, x_n is the observed value and z_n is the observational error. The Bayesian blocks algorithm proposed by Scargle, Norris, Jackson, and Chiang (2013) is a non- parametric method of segmenting time axis into non-uniform sub sequences or blocks. Continuous raw measurement x_i within each block is modelled using a piecewise constant model and mapped to a discrete value k_i . A partition of a time series of interval $\mathcal{T}$ is defined as the set of collection of blocks B_k which is exhaustive and without any overlap as shown in Eq. (3) and satisfies Eq. (4) and Eq. (5)

$$\mathcal{P}(I) = \{B_k : k = 1,2, \dots, n_k\} \quad (3)$$

$$I = \bigcup_k B_k \quad (4)$$

$$B_i \cap B_j = \emptyset \ \ for \ \mathrm{i} \neq j \quad (5)$$

To measure the fitness of partition $\mathcal{P}$, we define the fitness function as

$$F[\mathcal{P}(\mathcal{T})] = \sum_{k=1}^{n_k} f(B_k) \quad (6)$$

$f(B_k)$ is fitness of block B_k that measures how good the data is represented by the piecewise constant model in that block. In this paper, we have used standard normal distribution and likelihood maximization to model the process data within each block.

Bayesian blocks discretization uses dynamic programming approach to yield optimal partitions $\mathcal{P}^{opt}$.Consider a block B^{R+1} starting from cell r till cell $R+1$. If the fitness of the block is represented by$f'(r)$, then the fitness of partition $\mathcal{P}(R+1)$ as defined in Eq. (6) can be modelled as function of r:

$$A(r) = f'(r) + F[\mathcal{P}^{opt}(r-1)] \quad (7)$$

$$= f'(r) + \begin{cases} 0 & r = 1 \\ A(r-1) & r = 2,3, \dots, R+1 \end{cases}$$

For the range of r mentioned in Eq. (7), all the possible partitions $\mathcal{P}(R+1)$ are expressed and the optimal r can be easily found by maximizing

$$r^{opt} = argmax[A(r)] \quad (8)$$

Computations mentioned in Eq. (7) and Eq. (8) are carried out till $= \mathcal{T}$, giving us the optimal partition for the sequence $\mathcal{P}^{opt}(\mathcal{T})$.

3. PROPOSED METHODOLOGY

In this work, we propose a new methodology utilizing Bayesian Blocks discretization and Bayesian networks for RCI for faults and abnormal events in industrial systems. The main components of the proposed methodology are shown in Fig. 1 and comprise of fault detection and localization, data discretization and RCI modules.

3.1. Fault Detection and Localization

The fault detection and localization module detects process faults and identifies candidate variables carrying the signature of abnormal event/faults. In this work, we use principal component analysis (PCA) for fault detection and localization. PCA is a statistical procedure used for unsupervised dimensionality reduction and multivariate analysis (Deepthi and Rao 2014). It orthogonally transforms *n*-dimensional data into *k*-dimensions by projecting the data on to *k* principal directions of the data distribution known as principal components. Principal directions are obtained by calculating the eigenvectors of covariance matrix of the given

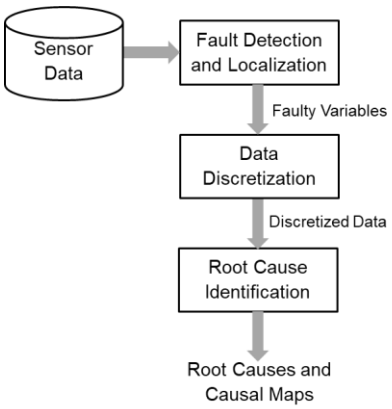

Figure 1. Proposed Methodology for Root Cause Identification

data. Eigenvectors with the highest eigenvalue are selected as principal components (Anand 2014). Hotelling's T^2 statistic is used to measure the variation of each sample within the PCA model. It is a generalized likelihood-ratio that gives the best fault detection rate (Chen et al. 2017; Mujica et al. 2011). Following is the procedure for fault detection and localization:

1. Let X = {x_1, x_2, x_3…. x_d} be an input vector of variables, I the identity matrix, Pc the number of principal components and $\sum$ the covariance matrix. T^2 can be calculated as:

$$T^2 = X^T Pc \sum^{-1} Pc^T X \quad (9)$$

2. T^2 values for all the process data are calculated and instances with T^2 values above the threshold are detected to be indicative of faulty/abnormal operation. T^2 statistic follows the Chi^2 distribution. To get threshold for T^2 statistics, the value of Chi^2 corresponding to 95% significance is obtained from the distribution

3. For instances identified to be faulty, Complete Decomposition Contributions (CDC) method is used for fault localization. T^2 score is decomposed using CDC method as summation of the contributions of each variable (Wise et al. 2009).

$$CDC_i^{T2} = (I_i^T Pc \sum^{-1} Pc^T X)^2 \quad (10)$$

4. CDC score for each variable for all the detected faulty instances is calculated.

5. For every faulty data instance, the particular variables for which the contribution exceeds the threshold are diagnosed as variables responsible for the fault.

3.2. Data Discretization

The variables diagnosed as faulty variables after fault detection and localization are discretized using Equal Width, Equal Frequency and Bayesian Blocks discretization techniques and fed to the RCI module.

3.3. Root Cause Identification

For each of the discretized datasets, causal maps are generated using Bayesian networks. A causal map is a directed graph that represents cause-effect relations. Each node in the causal map is a faulty variable while the edge between any two nodes represents the causal relationship between the two variables. To learn the structure of causal maps, Non-combinatorial Optimization via Trace Exponential and Augmented lagRangian for Structure learning (NOTEARS) algorithm is used (Zheng, Aragam, Ravikumar & Xing, 2018). Since searching the space for DAG structure is combinatorial, the search space increases exponentially as number of nodes increase, NOTEARS formulates the structure learning problem as a purely continuous optimization problem over real matrices that avoids this combinatorial constraint entirely. Using BNs, conditional probability distributions (CPDs) associated with each candidate variable are calculated. These CPDs are then used to learn the numerical parameters of causal maps.

The generated causal maps are used for studying the causal relationships among candidate variables and finding the root cause variable(s) (RCVs). In an acyclic causal map, the variable with only outgoing edges and no incoming edges is determined as the RCV. However, due to recycle streams and feedback control in industrial systems, causal maps often comprise of bidirectional edges and cyclic graphs. In such cases, potential RCVs are shortlisted from causal maps depending on the number of outgoing edges and process knowledge. Trend plots of the shortlisted variables are then analyzed to arrive at the RCVs.

4. CASE STUDY : TENNESSEE EASTMAN PROCESS

Tennessee Eastman process (TEP) is a simulation study of a chemical production by Downs and Vogel (1993). It is an industrial benchmark that is widely used in studies for process monitoring, time series data analysis and process fault detection and diagnosis (Aldrich 2019). The schematic of the process is shown in Fig. 2 (Russell, Chiang, & Braatz, 2000). The plant consists of 5 units: a reactor, a condenser, a stripper, a compressor and a separator. The reactions taking place in the reactor are given in Eq. (11). All the reactions are irreversible and exothermic in nature. Gaseous reactants A, D and E are fed to the reactor via separate streams. Stream 4 containing stripping agents is introduced to the stripper. It consists of reactants C and A, and an inert B. The overall reactor input consists of reactant streams A, D and E along with the recycle stream from the compressor (Stream 6). The recycle stream introduces element C into the reactor as well. The resulting mixture of product, unreacted gases and inerts from the reactor outlet are sent to the condenser where they are cooled before entering the vapor-liquid separator. In the separator, the vapor and liquid phases are separated. The condensate (liquid phase, Stream 10) is fed to the stripper while the vapor phase is recycled back to the reactor inlet after purging a part of it (Stream 9) to avoid inert accumulation. In the stripper, stripping agents extract the desired product (Stream 11) from the condensate which is then analyzed for its composition (XD, XE, XF, XG and XH) using the composition analyzer modules shown in Fig. 1.

$$\begin{cases} A(g) + C(g) + D(g) \rightarrow \mathrm{G(liq)} \\ A(g) + C(g) + \mathrm{E(g)} \rightarrow \mathrm{H(liq)} \\ A(g) + E(g) \rightarrow \mathrm{F(liq)} \\ 3D(g) \rightarrow \mathrm{2\ F(liq)} \end{cases} \tag{11}$$

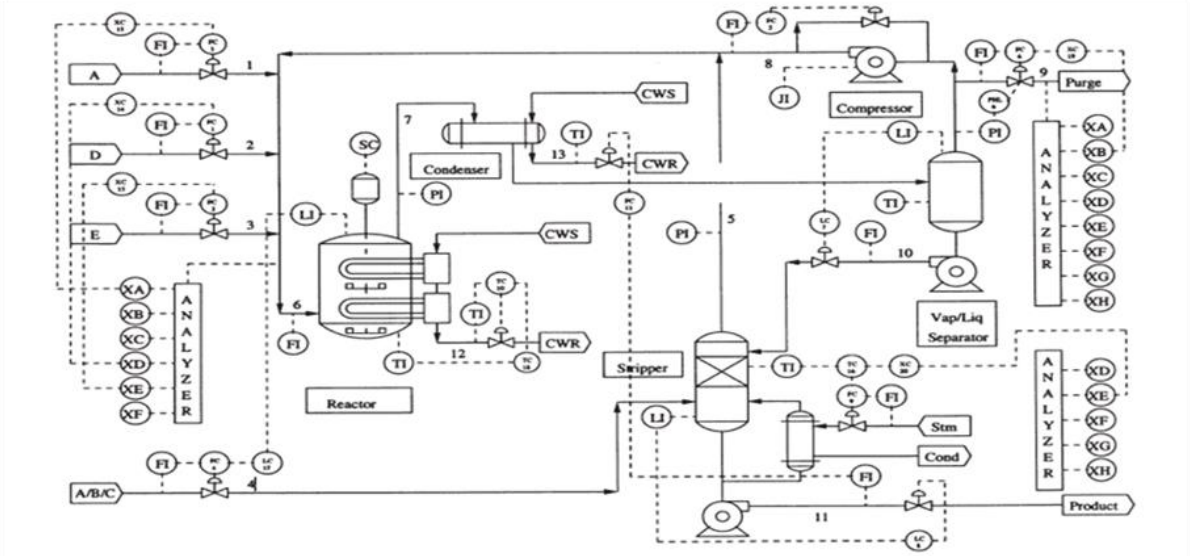

Figure. 2 Tennessee Eastman Process Flow Diagram (Russell, Chiang, & Braatz, 2000)

Variable	Description	Type	Variable	Description	Type
X1	A feed stream	MEAS	X27	Composition of E reactor feed	COMP
X2	D feed stream	MEAS	X28	Composition of F reactor feed	COMP
X3	E feed stream	MEAS	X29	Composition of A purge	COMP
X4	Total fresh feed stripper	MEAS	X30	Composition of B purge	COMP
X5	Recycle flow into reactor	MEAS	X31	Composition of C purge	COMP
X6	Reactor feed rate	MEAS	X32	Composition of D purge	COMP
X7	Reactor pressure	MEAS	X33	Composition of E purge	COMP
X8	Reactor level	MEAS	X34	Composition of F purge	COMP
X9	Reactor temp	MEAS	X35	Composition of G purge	COMP
X10	Purge rate	MEAS	X36	Composition of H purge	COMP
X11	Separator temp	MEAS	X37	Composition of D product	COMP
X12	Separator level	MEAS	X38	Composition of E product	COMP
X13	Separator pressure	MEAS	X39	Composition of F product	COMP
X14	Separator underflow	MEAS	X40	Composition of G product	COMP
X15	Stripper level	MEAS	X41	Composition of H product	COMP
X16	Stripper pressure	MEAS	X42	D feed flow valve	MV
X17	Stripper underflow	MEAS	X43	E feed flow valve	MV
X18	Stripper temperature	MEAS	X44	A feed flow valve	MV
X19	Stripper steam flow	MEAS	X45	Total feed flow stripper valve	MV
X20	Compressor work	MEAS	X46	Compressor recycle valve	MV
X21	Reactor cooling water outlet temp	MEAS	X47	Purge valve	MV
X22	Condenser cooling water outlet temp	MEAS	X48	Separator pot liquid flow valve	MV
X23	Composition of A reactor feed	COMP	X49	Stripper liquid product flow valve	MV
X24	Composition of B reactor feed	COMP	X50	Stripper steam valve	MV
X25	Composition of C reactor feed	COMP	X51	Reactor cooling water flow valve	MV
X26	Composition of D reactor feed	COMP	X52	Condenser cooling water flow valve	MV

Table 1. Process Variables

In this study, we demonstrate root cause identification using the proposed methodology for process faults in the Tennessee Eastman process. For this, we used the simulated data provided by Rieth, Amsel, Tran and Cook (2018). The dataset comprises of a total of 52 process variables with 22 of them being continuous process measurements (MEAS), 19 being composition measurements (COMP) and 11 being manipulated variables (MV) as listed in Table 1. Due to a significant time lag (6 to 15 minutes) in composition measurements (X23 to X41), they are omitted from causal inference analysis. The TE process is simulated for 20 faults of different nature such as a step fault, random variation in variables, slow drift of the process and sticking fault. The duration of each TE process simulation is 25 hours. During the simulations, the system is set to operate normally for 1 hour after which faults are introduced. Simulated data of all variables is collected every 3 minutes. Therefore, each simulation generates 500 data instances with the first 20 instances corresponding to normal operation and the rest 480 instances corresponding to faulty operation. In this work, we study faults given in Table 2. IDV (7) corresponds to faulty operation that occurred due to loss header pressure of reactant C in stream 4 which is the feed stream to the stripper unit. IDV (1) is caused due to step change in the A/C feed ratio in Stream 4.

Fault ID	Fault Description
IDV(7)	C Header pressure loss
IDV(1)	A/C Feed ratio, B Composition constant

Table 2. Fault ID and Description

5. RESULTS AND DISCUSSION

For detection and localization of both faults, PCA technique is used in the semi-supervised mode. 20000 data instances corresponding to normal operation are used for training and validation of the model. In the test data, instances for which the T2 score is above the threshold of 30.14 are detected to be faulty operating points. Faulty variables are diagnosed for the detected faulty instances using CDC. For each faulty instance, contributions of all variables to T2 are calculated and the mean of the contributions in the faulty instances is computed. Variables contributing to more than 5% of faulty instances are selected for root cause identification. These candidate variables are discretized and used for generating causal maps for the faults and subsequent root cause identification.

5.1. For IDV(7) fault

Application of the PCA model on IDV(7) fault data detected deviation from normal condition after 22 instances that can be observed from the change in the T^2 statistic in Fig. 3 (a). Confusion matrix for this fault is shown in Table 3. It can be observed from the table that the number of true positives and true negatives obtained from the PCA model are 479 and 20 respectively resulting in an accuracy of 99.79%.

	Predicted Faulty	Predicted Normal
Actual Faulty	479	1
Actual Normal	0	20

Table 3. Confusion Matrix for IDV (7)

Fault localization using CDC revealed 9 variables viz. X4, X7, X8, X13, X18, X19, X20, X45 and X50 which were identified as faulty variables in more than 5% of the total number of faulty instances as shown in Fig. 3(b). These variables are selected as candidates for RCI. Fault IDV(7) corresponds to faulty operation that occurred due to loss header pressure of reactant C in stream 4 which is the feed stream to the stripper unit. Due to this sudden drop in pressure, the total feed stripper flow rate (X4) dropped sharply which affects the stripper operation. This is evident from changes in several variables as shown in Fig 4. The stripper unit outputs stream 5 (recycle stream) to the reactor; thus the reactor level (X8) is also affected. The feedback controller tries to maintain the reactor level by manipulating the total feed flow stripper valve (X45) which adjusts the flow rate in Stream 4. IDV(7) is a complex fault that affected several units and process variables. However, knowing the origin of the fault, X4 can be considered to be the root cause variable. Fig. 5 shows the causal maps (CM) obtained using as-is numeric data (w/o discretization) and discretized data from the three discretization techniques viz. EWD, EFD and BBD on the candidate variables. In the CMs, the direction of the arrow indicates the direction of effect.

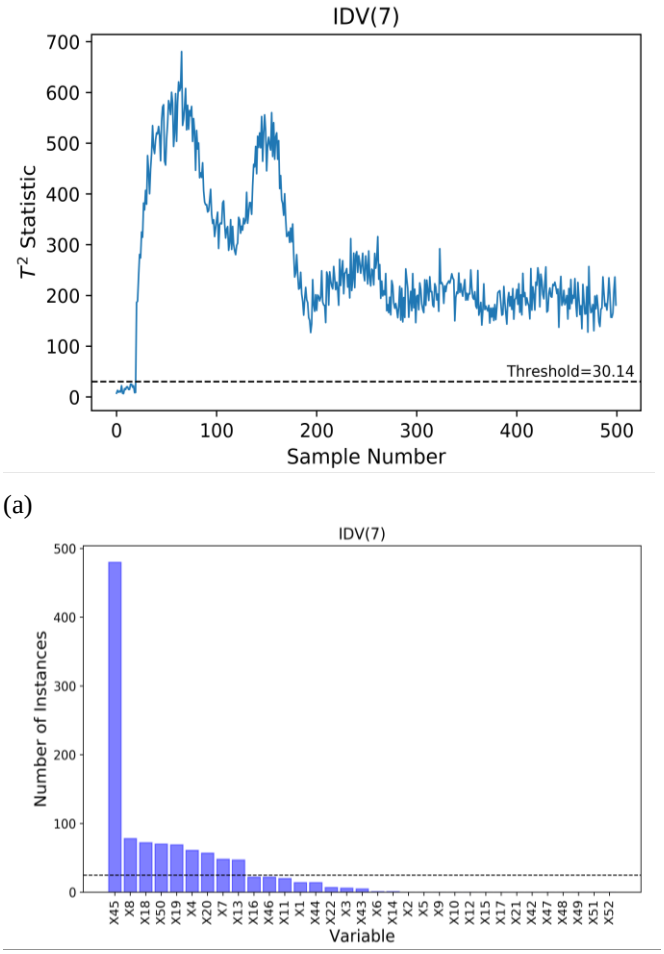

Figure 3. IDV (7) (a) Hotelling's T^2 plot (b) Variable contribution plot

The CM obtained with as-is data (Fig. 5a) has too many edges (33 in number) making it difficult to comprehend the causal relationships among the candidate process variables and diagnose the root cause variable. Further, it has several edges that are not physically not feasible, for example, total feed flow rate (X4) → Separator Pressure (X13). The large number of edges obtained is probably due to noisiness in the data. This emphasizes the need for coarse-graining of time series signals and reducing impact of dynamic noise on the causal model. CMs obtained using EW and EF discretized data are shown in Fig. 5 (b) and (c) respectively. There is a visible improvement in these CMs compared to the one

obtained using as-is data. The number of edges in the CMs generated using EWD and EFD data is 20 and 18 respectively. However, the cyclicity observed in these maps, for example, X4 → X13 → X19 → X45 → X4 in Fig. 5(b), leads to 7-8 potential root cause variables. In such a case, it is difficult to pinpoint the RCV without rigorous trend plot analysis to investigate the leading and lagging variables, and prior knowledge of the underlying fault. The CMs are also unable to capture the bi-directional edge between X4 and X45 variable, which is a manifestation of control action of X45 on X4. The CM obtained using BB discretized data is shown in Fig. 5(d). The number of edges in this CM is 16 which is 50% lower than the number of edges observed in the CM obtained from numeric data.

From this CM, X4 and X45 are identified to be potential root cause variables. However, since X45 is a manipulated variable that actually modulates X4, the root cause variable is identified to be X4 (i.e. Total fresh feed stripper feed flow rate). The causal edge X4 → X20 (compressor duty) is due to the varying composition of Stream 5, which changes compressor duty. Disturbances in reactor level (X8) and pressure (X7) can be seen to impact the manipulating flow control valve (X45) that modulates X4. We find that the root cause variable identified from the causal map generated using BB discretized data matches with that identified from process knowledge.

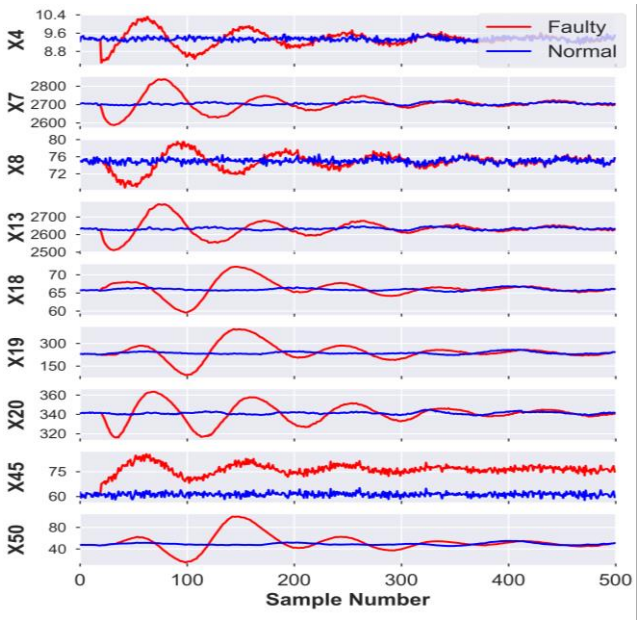

Figure 4. Trends of variables in IDV (7) showing normal & faulty operation

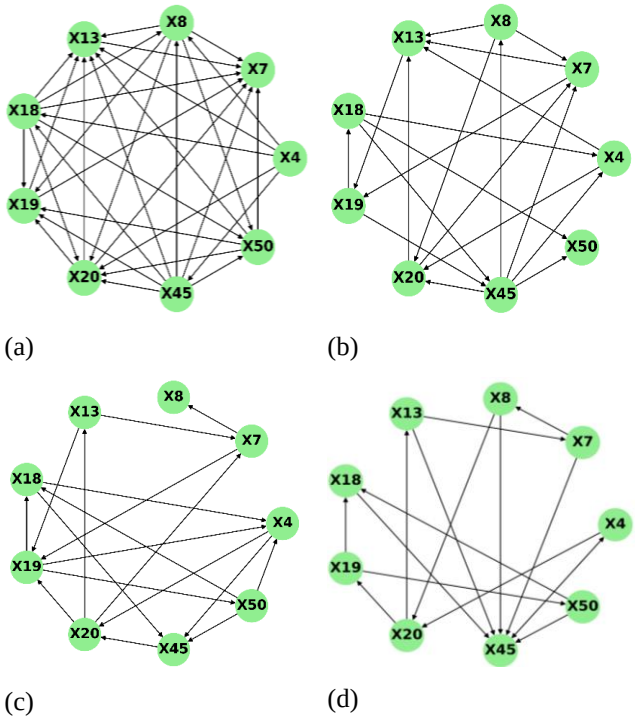

Figure 5. Causal Maps for IDV (7) obtained using (a) Numeric Data (b) EWD data (c) EFD data (d) BBD data

5.2 For IDV(1) fault

For the IDV (1) fault, the trend of T^2 statistic obtained using the PCA model is shown in Fig. 6(a) and confusion matrix is shown in Table 4. It can be observed from the table that the number of true positives and true negatives obtained from the PCA model are 471 and 20 respectively. The overall accuracy of fault detection for IDV(1) is 98.20%. The number of instances in which each of the variables are identified as contributing variables using CDC is shown in Fig 6(b). From the figures, it can be observed that 7 variables viz. X1, X4, X18, X19, X44, X45 and X50 are identified as faulty variables in at least 5% of the faulty instances and are selected as candidates for RCI.

	Predicted Faulty	Predicted Normal
Actual Faulty	471	9
Actual Normal	0	20

Table 4. Confusion Matrix for IDV (1)

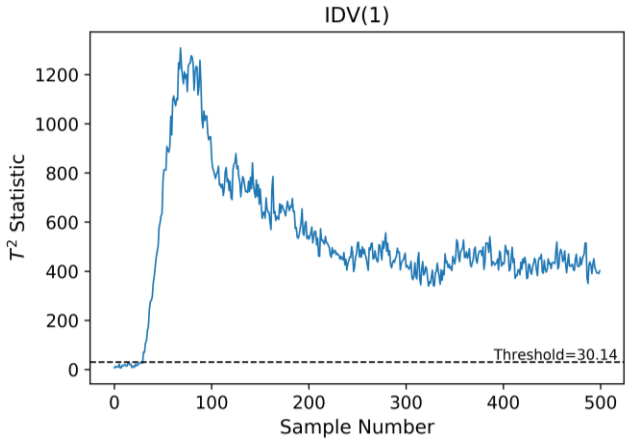

(a)

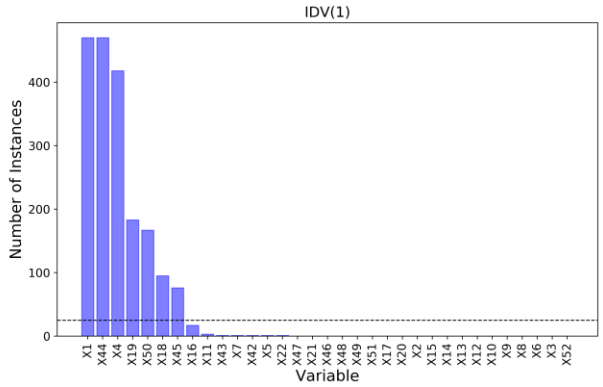

(b)

Figure 6. IDV (1) (a) Hotelling's T^2 plot (b) Variable contribution plot

IDV (1) is caused by step change in the ratio of reactants A to reactant C in Stream 4. This disturbance in the A/C feed ratio caused the recycle stream from stripper (Stream 5) and consequently the reactor input feed (stream 6) to have decreased percentage of reactant A. To counter this and maintain the composition of stream 6, the controller increased the input feed flow rate in Stream 1. The increase in reactant A feed flow rate (X1) can be seen in Fig. 7. The manipulated variable, X44 (reactant A feed flow valve) is used to modulate X1. Subsequently, the flow rates of stream 4 (X4) and stream 1 (X1) are modulated together to ensure that the total input of reactant A to the reactor remains the same. Since stream 4 is an input to the stripper, change in the A/C feed ratio in stream 4 affects several stripper variables (X18, X19 X45 and X50). While the change in the ratio of A/C in stream 4 is the origin of the process fault, since the ratio is not measured, there are no direct variables indicative of the fault. The nearest variables that have the fault signature are X4 and X1, and are considered to be RCVs for IDV (1).

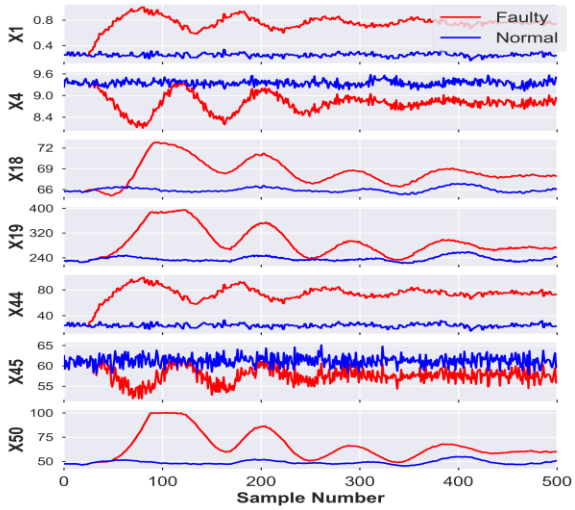

Figure 7. Trends of variables in IDV (1) showing normal & faulty operation

Fig. 8 shows the causal maps obtained for IDV(1) using numeric data as well as discretized data. The CM obtained using numeric data (Fig. 8(a)) has 15 edges and appears to have redundant edges, especially the ones reaching X44. From this CM, only X1 is identified to be the root cause variable. Figs. 8(b) and 8(c) show the CMs obtained using EWD and EFD data and have 12 and 13 edges respectively.

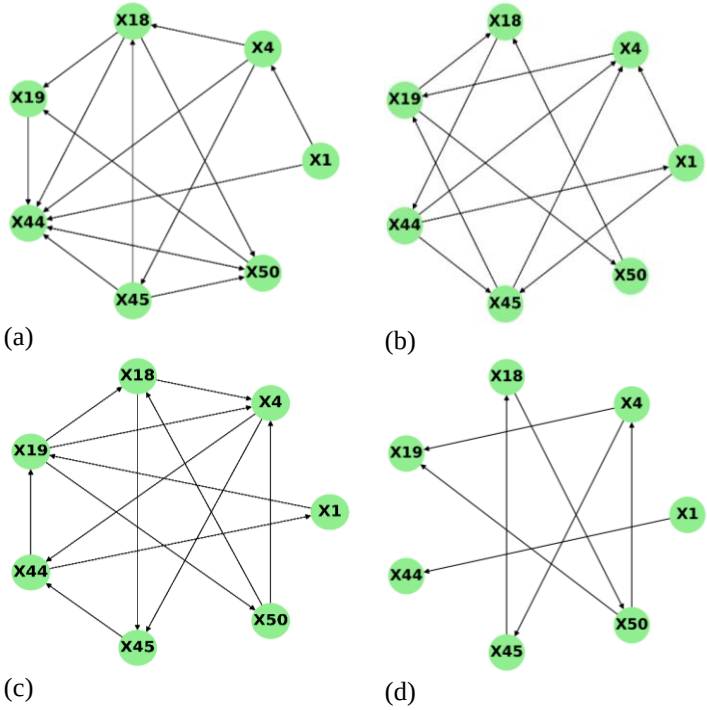

(a) (b) (c) (d)

Figure 8. Causal Maps for IDV (1) obtained using (a) Numeric Data (b) EWD data (c) EFD data (d) BBD data

From both the causal maps, only X1 can be identified as the root cause variable. It should also be noted that there are some spurious edges (e.g. X18 → X4) in Fig. 8(c). The CM obtained using BBD data is shown in Fig. 8(d) and has 7 edges which is ~50% lower than the number of edges in the CM obtained using numeric data. From this CM, X1 is a root cause variable as it has only one outgoing edge (X1 → X44) which is indicative of the control action of X44 on X1. While X4 has two outgoing edges and one incoming edge, the incoming edge (X50 → X4) is indicative of the indirect control action of X50 on X4. Therefore, X4 can also be identified as a root cause variable. In this fault as well, we find that the variables diagnosed to be root cause variables match with those identified from process knowledge.

In both faults, while the use of discretized data for learning Bayesian Networks significantly reduced the redundant edges compared to the numeric (as-is) data, the causal maps generated using EWD and EFD data had some spurious edges and did not always lead to the identification of the correct root cause variable(s). On the other hand, the use of BBD resulted in the generation of causal maps with physically logical edges and proper root cause identification. This highlights the effectiveness of using Bayesian Blocks as a discretization technique for RCI in complex industrial systems such as the Tennessee Eastman process.

6. CONCLUSION

In this study, we proposed a novel data-driven approach for identification of fault propagation and root causes in industrial systems. The approach consists of fault detection and localization using PCA models followed by generation of causal maps and root cause identification using Bayesian Networks. We studied the effect of data discretization using 3 methods viz. EW, EF and BB on causal map generation and efficacy of root cause identification from the generated maps. The proposed approach is demonstrated on two complex faults in the industrial benchmark Tennessee-Eastman (TE) process. We found that discretization of data reduces redundant nodes by up to 50%. We also found that the use of BB technique for discretization led to the successful identification of correct root causes of the faults compared to the other two techniques. The merits of the proposed method are: (1) It is a data-driven RCI approach that does not require a priori knowledge of the industrial process for causal map generation and (2) It is more effective in identification of the fault propagation paths and root causes in complex industrial systems compared to traditional methods. We plan to improve the approach using Dynamic Bayesian Networks.

REFERENCES

Aldrich, C. (2019). Process Fault Diagnosis for Continuous Dynamic Systems Over Multivariate Time Series. In Time Series Analysis—Data, Methods, and Applications. IntechOpen. doi: 10.5772/intechopen.85456

Anand, P. R. (2014). PCA Based Anomaly Detection. International Journal of Research in Advent Technology, 2(2), 5.

Chen, H.-S., Yan, Z., Zhang, X., Liu, Y., & Yao, Y. (2018). Root Cause Diagnosis of Process Faults Using Conditional Granger Causality Analysis and Maximum Spanning Tree. IFAC-PapersOnLine, 51(18), 381–386. doi: 10.1016/j.ifacol.2018.09.330

Chen, Z., Zhang, K., Shardt, Y. A. W., Ding, S. X., Yang, X., Yang, C., & Peng, T. (2017). Comparison of Two Basic Statistics for Fault Detection and Process Monitoring. IFAC-PapersOnLine, 50(1), 14776–14781. doi: 10.1016/j.ifacol.2017.08.2586

Deepthi, A. S., & Rao, V. K. (2014). Anomaly Detection Using Principal Component Analysis. International Journal of Computer Science And Technology.

Downs, J. J., & Vogel, E. F. (1993). A plant-wide industrial process control problem. Computers & Chemical Engineering, 17(3), 245–255. doi: 10.1016/0098-1354(93)80018-I

Kerber, R. (1992). ChiMerge: Discretization of numeric attributes. Proceedings of the Tenth National Conference on Artificial Intelligence, 123–128. San Jose, California: AAAI Press.

Lokrantz, A., Gustavsson, E., & Jirstrand, M. (2018). Root cause analysis of failures and quality deviations in manufacturing using machine learning. Procedia CIRP, 72, 1057–1062. doi: 10.1016/j.procir.2018.03.229

Mechraoui, A., Medjaher, K., & Zerhouni, N. (2008). Bayesian based fault diagnosis: Application to an electrical motor. IFAC Proceedings Volumes, 41(2), 7381–7386. doi: 10.3182/20080706-5-KR-1001.01248

Meel, A., O'Neill, L. M., Levin, J. H., Seider, W. D., Oktem, U., & Keren, N. (2007). Operational risk assessment of chemical industries by exploiting accident databases. Journal of Loss Prevention in the Process Industries, 20(2), 113–127. doi: 10.1016/j.jlp.2006.10.003

Mujica, L., Rodellar, J., Fernández, A., & Güemes, A. (2011). Q-statistic and T2-statistic PCA-based measures for damage assessment in structures. Structural Health Monitoring, 10(5), 539–553. doi: 10.1177/1475921710388972

Pearl, J. (1988). Probabilistic Reasoning in Intelligent Systems. Morgan Kaufmann.

Parsana, T. & Patel, M. (2014). A Case Study: A Process FMEA Tool to Enhance Quality and Efficiency of Manufacturing Industry. Bonfring International Journal of Industrial Engineering and Management Science. 4. 145-152. 10.9756/BIJIEMS.10350.

Rieth, C. A., Amsel, B. D., Tran, R., & Cook, M. B. (2018). Issues and Advances in Anomaly Detection Evaluation for Joint Human-Automated Systems. In J. Chen (Ed.), Advances in Human Factors in Robots and Unmanned

Systems (pp. 52–63). Cham: Springer International Publishing. doi: 10.1007/978-3-319-60384-1_6

Russell, E. L., Chiang, L. H., & Braatz, R. D. (2000). Data-driven Methods for Fault Detection and Diagnosis in Chemical Processes (M. J. Grimble & M. A. Johnson, Eds.). London: Springer London. https://doi.org/10.1007/978-1-4471-0409-4

Scargle, J. D., Norris, J. P., Jackson, B., & Chiang, J. (2013). STUDIES IN ASTRONOMICAL TIME SERIES ANALYSIS. VI. BAYESIAN BLOCK REPRESENTATIONS. The Astrophysical Journal, 764(2), 167. doi: 10.1088/0004-637X/764/2/167

Shu, Y., & Zhao, J. (2013). Data-driven causal inference based on a modified transfer entropy. Computers & Chemical Engineering, 57, 173–180. doi: 10.1016/j.compchemeng.2013.05.011

Wang, J., Yang, Z., Su, J., Zhao, Y., Gao, S., Pang, X., & Zhou, D. (2018). Root-cause analysis of occurring alarms in thermal power plants based on Bayesian networks. International Journal of Electrical Power & Energy Systems, 103, 67–74. doi: 10.1016/j.ijepes.2018.05.029

Wise, B. M., Gallagher, N. B., Bro, R., Shaver, J. M., Windig, J., & Koch, R. S. (2009). PLS_Toolbox. Eigenvector Research, Inc.

Wollstadt, P., Martínez-Zarzuela, M., Vicente, R., Díaz-Pernas, F. J., & Wibral, M. (2014). Efficient Transfer Entropy Analysis of Non-Stationary Neural Time Series. PLOS ONE, 9(7), e102833. doi: 10.1371/journal.pone.0102833

Zhao, G.-Q., Wang, J.-G., Chen, Z., Yao, Y., & Xu, C. (2020). Causal Network Analysis and Root Cause Detection Based on Parameter Variable Sequence Transfer Entropy. 2020 IEEE 9th Data Driven Control and Learning Systems Conference (DDCLS), 783–788. doi: 10.1109/DDCLS49620.2020.9275041

Zheng,X., Aragam, B. , Ravikumar, P. & Xing E. P. (2018). DAGs with NO TEARS: Continuous Optimization for Structure Learning. arXiv:1803.01422v2 [stat.ML]